Development of a new slurry coating design for the surface protection of gas turbine components

Benjamin Grégoire, Gilles Bonnet, Fernando Pedraza

Development of a new slurry coating design for the surface protection of gas turbine components

Benjamin Grégoire*, Gilles Bonnet, Fernando Pedraza

Laboratoire des Sciences de l'Ingénieur pour l'Environnement (LaSIE, UMR-CNRS 7356), Université de La Rochelle, Avenue Michel Crépeau, 17042 La Rochelle Cedex 1, France

* Corresponding author: benjamin.gregoire@univ-lr.fr

ABSTRACT

A new slurry coating design incorporating a first layer of Cr microparticles at the substrate surface and a surmounting second layer of Al microparticles to enrich the substrate with Al was investigated. The microstructure of the coating was tailored by adjusting the initial thicknesses of Cr and Al layers. The intermediate layer of Cr microparticles acted as a barrier to molten Al by forming Al-Cr intermetallic compounds thereby suppressing the highly exothermic reactions usually observed between molten Al and nickel-based materials. This also significantly decreased the inward diffusion rate of Al towards the substrate at 700°C. Annealing at 1100°C then promoted the outward diffusion of nickel atoms from the substrate and their combination with Al from the synthesized Al-Cr intermetallic phases compounds resulting in the direct formation of β-NiAl with expelled Cr. The mechanisms of formation of the diffusion layers and the influence of Cr on the aluminizing progress are discussed.

Keywords: Superalloys; Intermetallics; Slurry coatings; Aluminizing; Diffusion

1. Introduction

Most gas turbine components are composed of nickel-based superalloys because their improved γ-γ' microstructure and optimized chemical composition provide high creep and fatigue resistance at elevated temperatures. However, nickel-based superalloys suffer from oxidation and hot corrosion in service when submitted to corrosive atmospheres [1,2]. This led to the development of protective coating systems that significantly improve service lifetimes. A wide range of desirable features is usually considered for the coating systems including low rates of scale formation, high concentration of scale forming elements (i.e. a reservoir of such elements) and limited compositional and mechanical changes of the substrate [3].

In this perspective, aluminium diffusion coatings are applied for decades to improve the environmental resistance of gas turbine components [1,3-7]. These coatings are based upon the Al enrichment of the surfaces to produce an Al reservoir constituted of the β-NiAl intermetallic compound [1,4]. The high Al content promotes the selective oxidation of Al at high temperatures forming a dense, adherent and slow-growing alumina scale on the surface [8,9]. When local

breakage or spallation of the alumina scale occurs, Al diffuses outwardly from the coating and combines with oxygen to heal the scale. Whereas aluminium diffusion coatings are particularly performant to fight against oxidation up to 1100°C [10], modified aluminide coatings are usually preferred when additional resistance is required. This modification includes Cr and/or Si for hot corrosion resistance [5,11-15] and Pt for cyclic oxidation resistance at temperatures above 1100°C [7,10,16-19].

Depending on the thermodynamic activity of Al, different coating microstructures can be obtained on nickel-based superalloys. They are usually classified as low-temperature high-activity (LTHA) and high-temperature low-activity (HTLA) microstructures [1,4,6] but mixed coating growth is also reported in literature [20,21]. The mechanisms of formation of aluminide coatings first proposed by Goward and Boone [1,4] are confirmed with diffusion models [22,23]. When the Al source is rich in Al (LTHA), the inward diffusion of Al brings about the formation of δ-Ni_2Al_3 at the substrate surface. Since the diffusivity of Al is much higher than that of Ni in the δ-Ni_2Al_3 phase [23], Al further diffuses inward and the initial surface of the substrate remains at the outermost surface upon aluminizing. Consequently, slowly-diffusing alloying elements and substrate carbides are trapped in the δ-Ni_2Al_3 coating matrix. A further annealing is usually carried out at about 1000-1100°C to transform the brittle δ-Ni_2Al_3 phase into the desired β-NiAl phase [4,18]. By decreasing the thermodynamic activity of Al and performing the aluminizing at high temperature (HTLA), the coating grows by major outward diffusion of Ni. This drives to the direct formation of Ni-rich β-NiAl phase in which the diffusivity of Ni is higher than that of Al [23]. The outward motion of Ni to combine with Al results in the formation of a clean β-NiAl additive layer above the initial surface of the substrate. Simultaneously, an interdiffusion zone (IDZ) forms in the substrate by depletion of Ni and precipitation of slowly-diffusing elements. Low-activity coatings exhibit higher oxidation resistance than high-activity coatings since a clean β-NiAl phase free of precipitates and carbides is formed [18,24].

Aluminide coatings are generally produced by pack cementation [4,6,12,14,25-27], out-of-pack [6,12,28-30] or slurry processes [6,4,15,31]. Because of the environmental constraints of pack cementation and of out-of-pack related to the use of halides and other hazardous chemicals, significant efforts have been made over the past years to apply water-based slurry coatings [32-39]. In addition to being free of chromates, phosphates and halide activators, they are very cheap and easy to tailor including the co-deposition of Si, Cr and other elements to Al [40-43].

The mechanisms of formation of Al-containing water-based slurry coatings have already been described on pure nickel [34,35] and nickel-based superalloys [44]. They involve self-propagating high-temperature synthesis (SHS) following wetting and dissolution of the nickel-based material into molten Al and subsequent inward diffusion of Al to form Al-rich nickel

aluminides (i.e. $NiAl_3$ and Ni_2Al_3). When the Al reservoir is consumed, solid-state diffusion occurs resulting in a pure high-activity coating with a sintered network of alumina shells [35,44]. Nevertheless, low-activity coatings were successfully obtained by Montero et al. using mixtures of Al and pre-alloyed Cr-Al powders [36,41]. The influence of Cr on the control of the aluminizing process was demonstrated in Ref. [45] by differential scanning calorimetry (DSC) and thermogravimetric analyses. Layering of Al and Cr particles allowed to form Al_xCr_y intermetallic compounds that in turn controlled the Al activity on pure nickel substrates [43].

In this study, polycrystalline Ni20Cr was employed as a model alloy to investigate the influence of Cr upon aluminizing [27,46-49] before extrapolation to CM-247 LC superalloy. The carbides originally present in the CM-247 LC superalloy have been considered as natural markers to identify the coating growth direction upon aluminizing [20]. Their position highlighted the aluminizing reaction front and the position of the initial surface of the substrate prior to aluminizing.

2. Experimental procedure

The nominal chemical compositions of the polycrystalline Ni20Cr and of the directionally-solidified CM-247 LC superalloy are listed in **Table 1**. Coupon samples of approximately 2.0 mm thickness were prepared from Ni20Cr (GoodFellow) and CM-247 LC (provided by Siemens) cylindrical rods, with respective diameters of 12.0 and 20.0 mm. SiC P180 paper was then used to prepare the surfaces of the samples. The polished samples were finally rinsed with deionized water and cleaned in ethanol before slurry deposition.

Table 1. Nominal composition (wt.%) of the two nickel-based materials investigated in this study.

	Ni	Cr	Al	Si	Ti	Co	Mo	Hf	Ta	W	C	B
Ni20Cr	Bal.	20.0	-	1.5	-	-	-	-	-	-	-	-
CM-247 LC	Bal.	8.1	5.6	-	0.7	9.2	0.5	1.4	3.2	9.5	0.07	0.015

The slurry formulation included a 1/10 PolyVinyl Alcohol (PVA)/deionized water solution to which spherical powders of Al (2-15 µm, Sibthermochim, Russia) or flake-like powders of Cr (2-10 µm, Goodfellow) were added. After blending, the slurries were deposited by air brush on the coupon samples. The new slurry coating design, referred to as the Cr/Al double-layer system included the deposition of a first layer of Cr microparticles over the substrate and a second layer of Al microparticles on top. Reference samples slurry coated with Al microparticles were also prepared to highlight the influence of Cr on the slurry aluminizing of Ni20Cr and CM-247 LC nickel-based superalloy. The samples were systematically let to dry at room temperature for 1 h in lab air after each slurry deposition [33]. The samples were periodically weighed with a 10^{-4} g precision balance to control the deposited slurry quantity and the Cr/Al ratio. Since the initial Cr/Al ratio was found to influence the course of the exothermic reactions and the stoichiometry of the synthesized intermetallic compounds [43,45], different chemical compositions (i.e. mass of both Cr and Al layers) were investigated. **Table 2** summarizes the compositions (given in wt.%) and the corresponding deposited slurry quantity and dry coating thickness investigated in this study on both Ni20Cr and CM-247 LC superalloy.

Table 2. Summary of the different slurry systems investigated in this study with the corresponding deposited slurry quantity and the dry coating thickness for both Cr and Al layers.

Double-layer system (wt.%)	Deposited slurry quantity ($mg.cm^{-2}$)	Dry coating thickness (µm)
33Cr/67Al	5/10	12/50
40Cr/60Al	6/9	15/45
50Cr/50Al	10/10	25/50
56Cr/44Al	10/8	25/40

Up to ten samples were simultaneously annealed in a conventional horizontal furnace (quartz tube) to form the diffusion coatings. After introduction of the samples, the reaction chamber was sealed and purged with a vacuum pump down to approximately 0.2 mbar. The reaction chamber was then filled with argon at a pressure slightly over the atmospheric pressure and was ventilated with a flow of argon during the aluminizing heat treatment to prevent any significant oxidation of the metallic substrates and of the microparticles. The reference two-step high-activity heat treatment consisted of a diffusion step at 700°C for 2 h to foster the inward diffusion of Al towards the substrate and of an annealing step at 1100°C for 2 h to promote interdiffusion between Al and Ni and to stabilize the β-NiAl phase [34,35]. Note that a first step at 400°C for 1 h was systematically carried out prior to aluminizing to decompose the organic binder (i.e. PVA) [33]. The heating ramps were fixed at 5°C/min and the samples were naturally cooled down to room temperature at the end of the annealing treatment. Additional samples were exposed only to the diffusion step (700°C-2 h) to elucidate the mechanisms of formation.

Surface and cross-section of the slurry coated samples were characterized by light optical microscopy (LEICA DMRM microscope equipped with a LEICA MC170 HD camera) and a FEI Quanta 200F environmental SEM. The SEM observations were performed in low vacuum (0.9 mbar) and at 20 kV. Energy Dispersive X-ray Spectroscopy (EDS) was performed to analyse the chemical composition of the constitutive intermetallic phases and oxides (EDAX detector coupled to the SEM). This technique also generated X-ray maps of the diffusion layers to give the spatial distribution of the elements. For cross-section observations, the samples were embedded in an epoxy resin and progressively ground with finer SiC papers down to P4000 grade (median diameter of 2.5 μm) then polished with a 1 μm water-based diamond suspension (Struers). A final polishing with a colloidal silica suspension (Struers OP-S 0.04 μm) was performed to better reveal the microstructure of the diffusion layers and of the nickel-based materials.

3. Results

3.1. Slurry aluminizing of Ni20Cr

3.1.1. From Al microparticles

Ni20Cr was first aluminized with Al microparticles in flowing Ar (**Fig. 1**). After the diffusion heat treatment, diffusion spots are randomly observed together with uncoated areas on the surface of the substrate (**Fig. 1**a). At higher magnification (**Fig. 1**b), the BSE mode highlights the uneven reaction front between the aluminized layers (dark contrast) and uncoated areas. The comparison between the EDS analyses and the theoretical phases of the Al-Ni-Cr ternary phase diagrams at 700°C and at 1100°C is given in **Table 3**. After the diffusion heat treatment, the diffusion islands mostly consist of a δ-Ni_2Al_3 matrix with precipitation of Cr-rich phases whose composition most likely corresponds to Al_8Cr_5 according to the microstructures presented in Ref. [47] and the Al-Ni-Cr ternary diagram at 700°C [50,51]. The composition of the outer region of the diffusion islands falls in a three-phase domain [50]. The cracks observed through the intermetallic phases of the diffusion layers are most likely due to the metallographic preparation

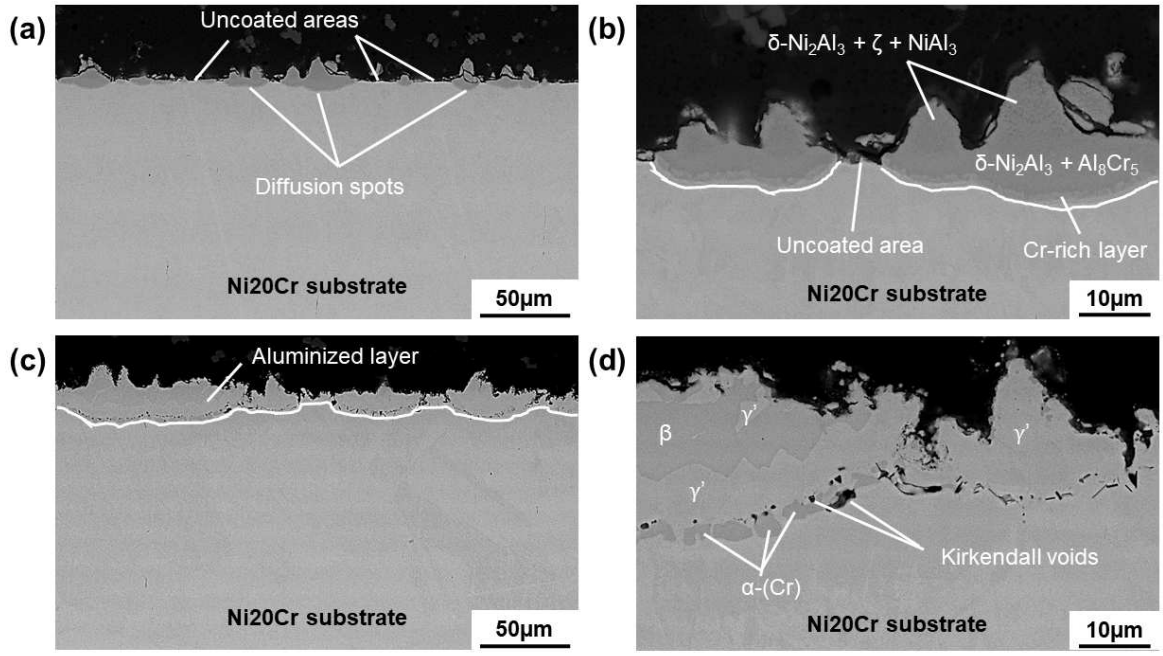

Fig. 1. BSE cross-section images of the diffusion layers formed on Ni20Cr slurry coated with Al microparticles after **(a)**, **(b)** 400°C-1 h + 700°C-2 h and **(c)**, **(d)** 400°C-1 h + 700°C-2 h + 1100°C-2 h in flowing Ar. **(b)** and **(d)** are magnified views of **(a)** and **(c)**, respectively.

of the brittle δ-Ni_2Al_3 coating matrix [52].

After the complete heat treatment (**Fig. 1**c), the aluminized layer is uneven and the sample exhibits a rough surface. Similar microstructures were reported by Rannou et al. for the aluminizing of Ni20Cr from Al-containing water-based slurries [49]. The diffusion layers are

composed of both β-NiAl and γ'-Ni_3Al phases with, respectively, about 8 and 6 at.% of dissolved Cr (**Table 3**). The transformation of δ-Ni_2Al_3 into β-NiAl and γ'-Ni_3Al phases and the formation of Kirkendall voids at the interface between the Al reservoir and the substrate strongly support that outward diffusion of nickel occurred at 1100°C [27]. Because of the limited solubility of Cr in β-NiAl and in γ'-Ni_3Al [50,53], the excess of Cr was rejected at the interface between the Ni_xAl_y phases and the Ni20Cr substrate in the form of α-(Cr) (**Fig. 1**d). This suggests that the formation of a Cr-rich layer at the boundary between the aluminide layer and the substrate acted as a barrier of diffusion preventing further Al ingress into the substrate.

Table 3. Average chemical composition of the individual phases observed in the diffusion layers (cf. **Fig. 1**) after the diffusion and the complete heat treatment measured by EDS (at.%). The composition range of the ternary ζ-phase is about $Al_{74}Ni_8Cr_{18}$ [50].

Heat treatment	Phase domain	Al	Si	Cr	Ni	Ref.
700°C-2 h	δ-Ni_2Al_3 + ζ-phase + $NiAl_3$	68.9	-	6.3	24.8	[50,51]
	δ-Ni_2Al_3 + Al_8Cr_5	58.5	-	9.1	32.4	[50,51]
700°C-2 h + 1100°C-2 h	β-NiAl	34.9	1.6	7.8	55.7	[54,55]
	γ'-Ni_3Al	24.3	2.5	6	67.2	[54,55]
	α-(Cr)	2.9	1.1	74.2	21.8	[54]

3.1.2. From the Cr/Al double-layer system

The BSE cross-section images of Ni20Cr coated with the Cr/Al double-layer system are given in **Fig. 2**. After the diffusion heat treatment at 700°C (**Fig. 2**a and **Fig. 2**b), Al and Cr microparticles reacted forming Al_xCr_y intermetallic compounds (IMCs) in the slurry deposit whereas unreacted Cr microparticles are still observed on top of the substrate. The composition of these phases ranges from $Al_{79.5}Ni_{2.9}Cr_{17.6}$ to $Al_{78.3}Ni_{4.5}Cr_{17.2}$ (at.%), which corresponds to the Al_4Cr + ζ-phase domain (Al_4Cr only dissolves up to 1 at.% of Ni) [50]. The Cr interlayer considerably hampered Al inward diffusion towards the substrate as previously reported on pure nickel [43]. After the additional step at 1100°C for 2 h (**Fig. 2**c), a continuous aluminized layer grew on the Ni20Cr substrate whereas slurry residues (i.e. the synthesized intermetallic compounds acting as Al donors) are still observed on top of the aluminized layer. **Fig. 2**d shows the microstructure of the aluminized layer and the corresponding EDS concentration profile is presented in **Fig. 3**. Three different layers can be distinguished: a 6-7 μm thick IDZ with Kirkendall porosity, an intermediate 20 μm thick β-NiAl layer and an outer Al-rich β-NiAl layer of approximately 10 μm with undissolved Cr.

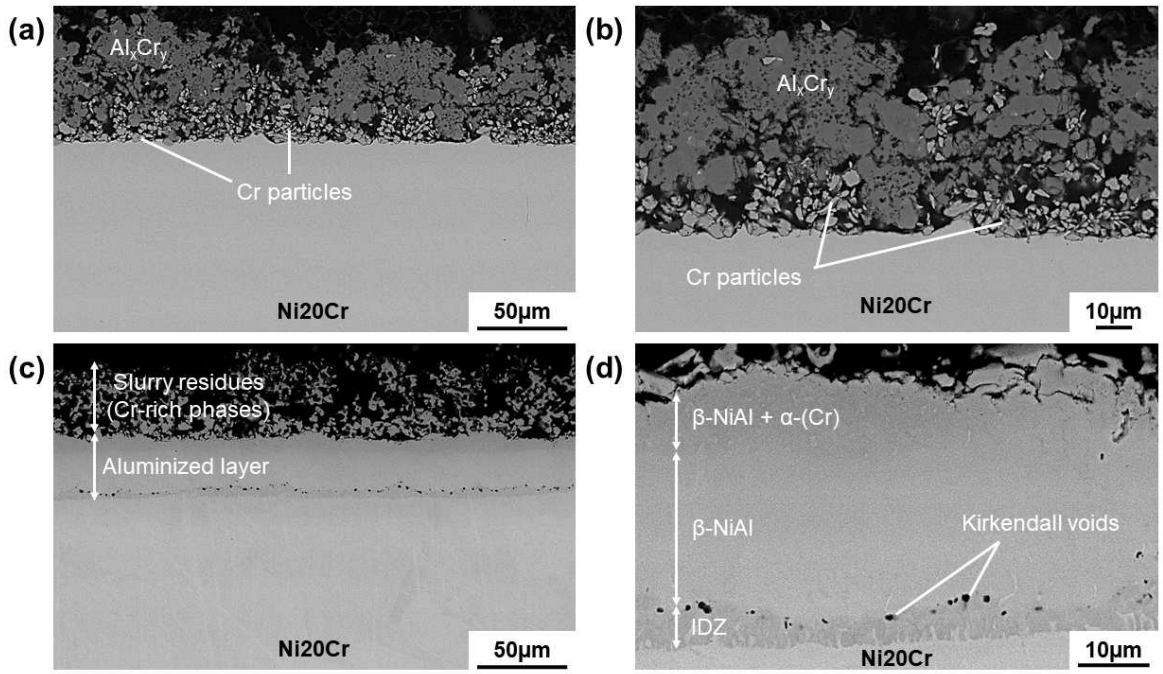

Fig. 2. BSE cross-section images of the diffusion layers formed on Ni20Cr coated with the 50Cr/50Al double-layer system after **(a)**, **(b)** 400°C-1 h + 700°C-2 h and **(c)**, **(d)** 400°C-1 h + 700°C-2 h + 1100°C-2 h in flowing Ar.

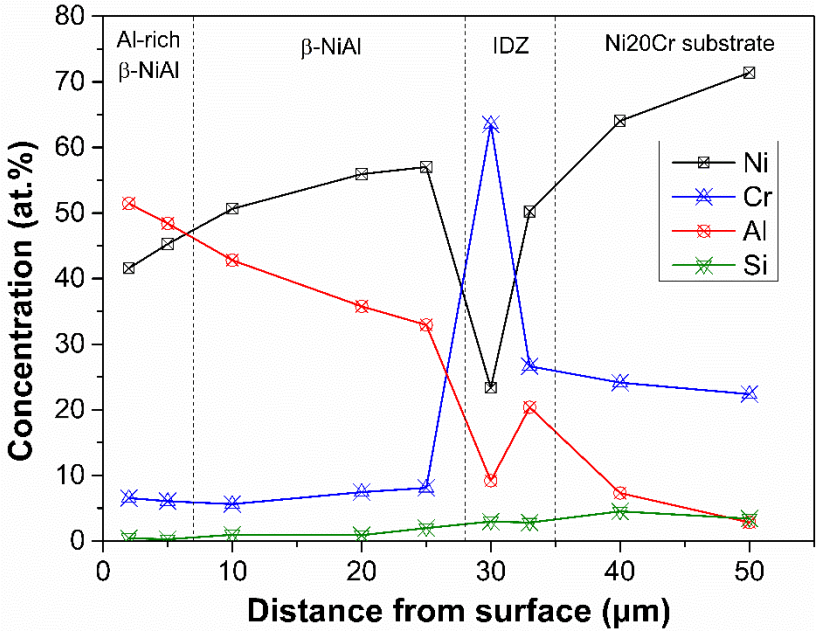

Fig. 3. EDS concentration profiles of Ni, Cr, Al and Si across the diffusion coating formed on Ni20Cr after 400°C-1 h + 700°C-2 h + 1100°C-2 h in flowing Ar (cf. **Fig. 2**d).

To highlight the influence of the initial Cr/Al ratio (i.e. deposited masses of Cr and Al slurries) on the final microstructure of the diffusion coatings, two compositions were tested (50Cr/50Al and 40Cr/60Al in wt.%). The cross-section images of the diffusion coatings formed after the complete heat treatment are given in **Fig. 4**. Unlike **Fig. 1**c, continuous and even diffusion layers are formed on Ni20Cr substrate for both compositions. This underlines the beneficial influence of the Cr interlayer on the control of the aluminizing process. Light optical microscopy allowed to better differentiate Al-rich hyperstoichiometric (blue to purple colour) and Ni-rich hypostoichiometric (yellow to brown colour) β-NiAl [56,57]. Irrespective of the initial Cr/Al ratio, the diffusion coatings present a thin IDZ with Kirkendall porosity, an intermediate β-NiAl layer and an outer Al-rich β-NiAl layer with undissolved Cr microparticles (bright contrast with light optical microscopy). The major difference between the diffusion coatings presented in **Fig. *4*** lies in the thickness of the Al-rich β-NiAl layers. The greater the Al content of the slurry deposit, the thicker the Al-rich β-NiAl layer after aluminizing. Similar conclusions were reported by Tu and Seigle by varying the pack composition (Al donor) for the aluminizing of various Ni-Cr alloys [46]. The Cr-rich phases observed above the diffusion layers in **Fig. 4**a and **Fig. 4**b resulted from the depletion of Al from the Al-Cr phases synthesized at low temperature (**Fig. 2**a).

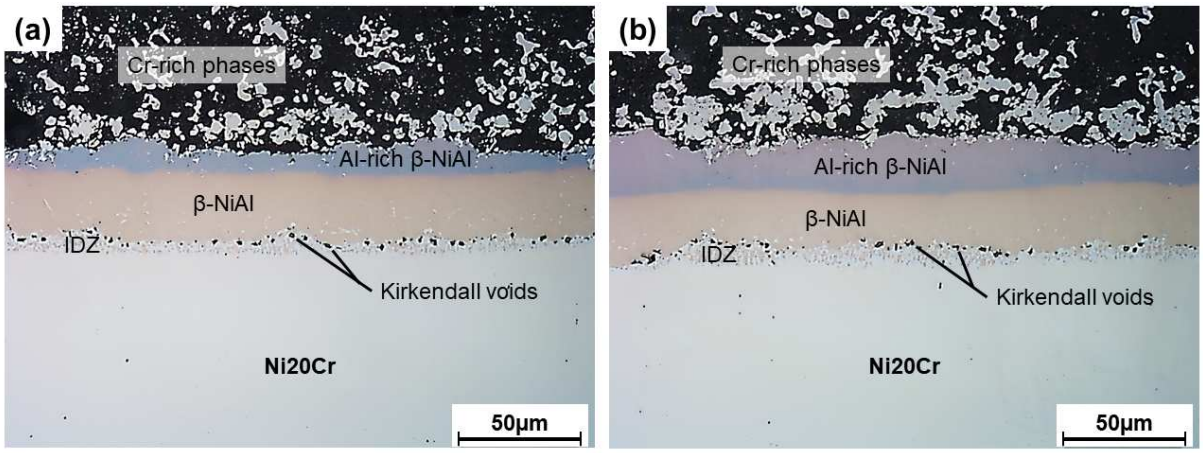

Fig. 4. Light optical micrographs of the **(a)** 50Cr/50Al and **(b)** 40Cr/60Al double-layer systems elaborated on Ni20Cr after 400°C-1 h + 700°C-2 h + 1100°C-2 h in flowing Ar.

3.2. Slurry aluminizing of CM-247 LC superalloy

3.2.1. From Al microparticles

The CM-247 LC superalloy was first slurry coated with Al microparticles and submitted to the complete heat treatment to produce a reference high-activity coating (**Fig. 5**a). The coating is divided in three distinct layers: a ceramic top coat composed of hollow Al_2O_3 spheres, a thick Al-rich diffusion layer (**Fig. 5**b) with fine precipitates and a thin IDZ (interdiffusion zone) with coarse precipitates. Such microstructure is characteristic of high-activity slurry coatings [35,37,38]. Substrate carbides are observed through the diffusion layer and at the surface of the coating layer demonstrating that the coating formed by singular inward diffusion of Al into the CM-247 LC superalloy [1,20]. The initial surface of the substrate therefore remained at the extreme surface of the coating layer upon aluminizing [20]. The abundance of fine precipitates within the diffusion layer also confirmed the major inward diffusion of Al since the substrate elements were trapped in the outer region of the coating [1,20,27,36].

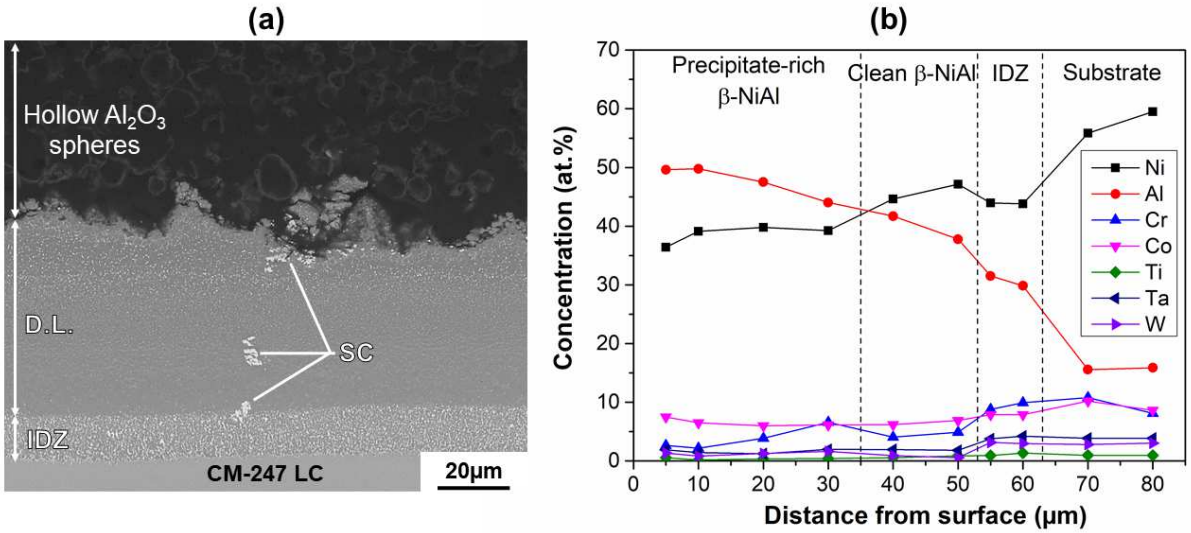

Fig. 5. (a) BSE cross-section image and **(b)** corresponding EDS concentration profile of CM-247 LC slurry coated with Al microparticles after 400°C-1 h + 700°C-2 h + 1100°C-2 h in flowing Ar. D.L.: diffusion layer, IDZ: interdiffusion zone and SC: substrate carbide.

3.2.2. From the Cr/Al double-layer system

Fig. 6a and **Fig. 6**b present the coating microstructures obtained on CM-247 LC after the complete heat treatment for, respectively, the 56Cr/44Al and the 33Cr/67Al double-layer systems. For both compositions, the microstructures include an aluminized layer and a layer with Cr-rich phases resulting from the Al depletion of the synthesized Al-Cr intermetallic compounds [43]. The position of the substrate carbides through the coating layers highlights that different mechanisms of formation have been involved [20]. For the 56Cr/44Al double-layer system (**Fig. 6**a), the substrate carbides remained in the interdiffusion zone suggesting that the outer region of the coating (i.e. additive layer) formed above the surface of the substrate. This resulted in a diffusion coating with an IDZ/A.L. thickness ratio close to one, typical of low-activity microstructures [4,36]. The distribution of bright phases through the additive layer suggests the presence of undissolved Cr particles according to EDS spot analyses. Based on the EDS concentration profile (**Fig. 7**a), the additive layer is based on Al-rich β-NiAl whereas the interdiffusion zone is based on Ni-rich β-NiAl. Note that the EDS spot analyses performed in the additive layer were done in the coating matrix (i.e. aluminide phase) and, therefore, that the mean Cr concentration of the additive layer is higher than the values given in **Fig. 7**a . The colour difference observed in light optical microscopy between the additive layer and the interdiffusion zone (**Fig. 6**a) is therefore associated with the Al concentration gradient of the β-NiAl phase [56,57]. Similar microstructures were observed by Streiff and Boone for a low activity two-step

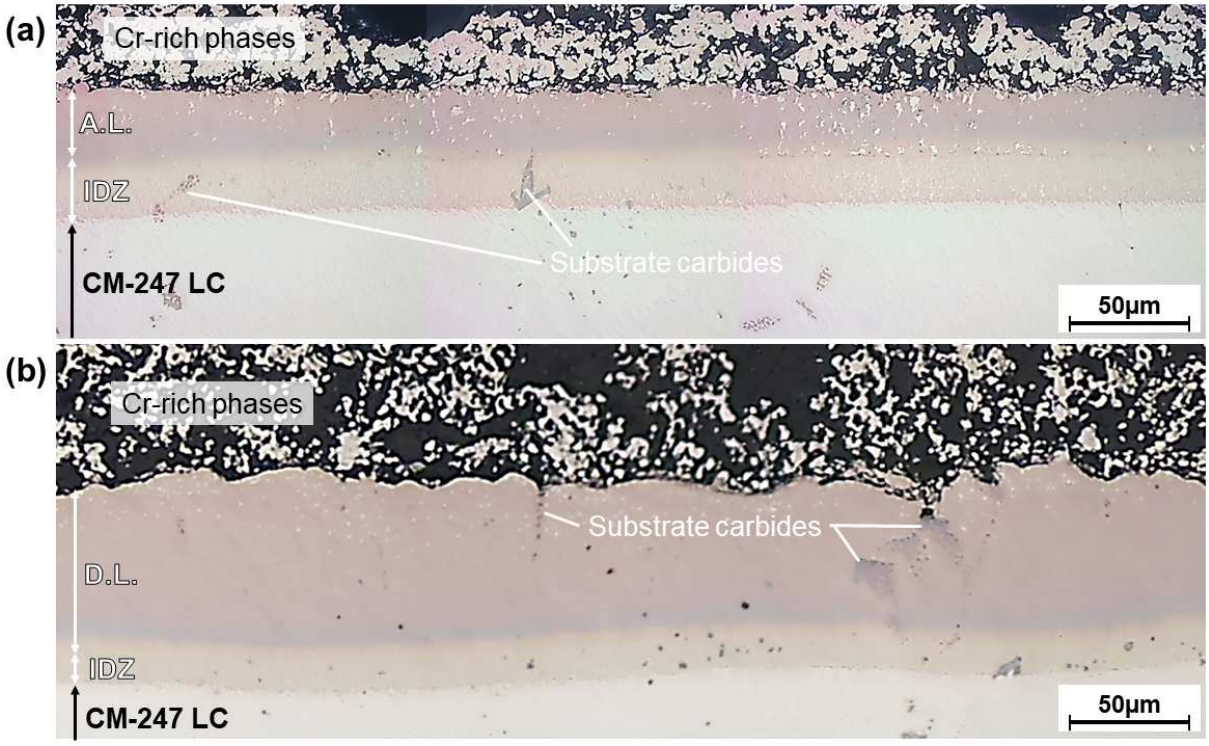

Fig. 6. Cross-section optical micrographs of the **(a)** 56Cr/44Al and **(b)** 33Cr/67Al double-layer systems elaborated on CM-247 LC superalloy after 400°C-1 h + 700°C-2 h + 1100°C-2 h in flowing Ar. A.L.: additive layer.

chromizing-vapour phase aluminizing process [5].

For the 33Cr/67Al double-layer system (**Fig. 6**b), the coating microstructure is significantly different. Like with **Fig. 5**a, the substrate carbides are located across the whole thickness of the coating suggesting that the initial surface of the substrate remained at the outermost surface of the coating layer upon aluminizing [20]. The overall thickness of the aluminized layer is of approximately 80 µm with an IDZ/D.L. thickness ratio of about 0.2. The EDS concentration profile of the aluminized layer is given in **Fig. 7**b. The diffusion layer is based on Al-rich β-NiAl with about 5 at.% Cr and local W enrichments typical of inwardly-growing coating [20,27]. Note that the EDS measurements of the diffusion layer were done in the coating matrix (i.e. aluminide phase) to highlight the Al concentration gradient. The formation of a relatively thin IDZ suggests that outward diffusion of nickel occurred at 1100°C. The Al reservoir formed with the 33Cr/67Al double-layer system is thus significantly larger than that obtained with the 56Cr/44Al one.

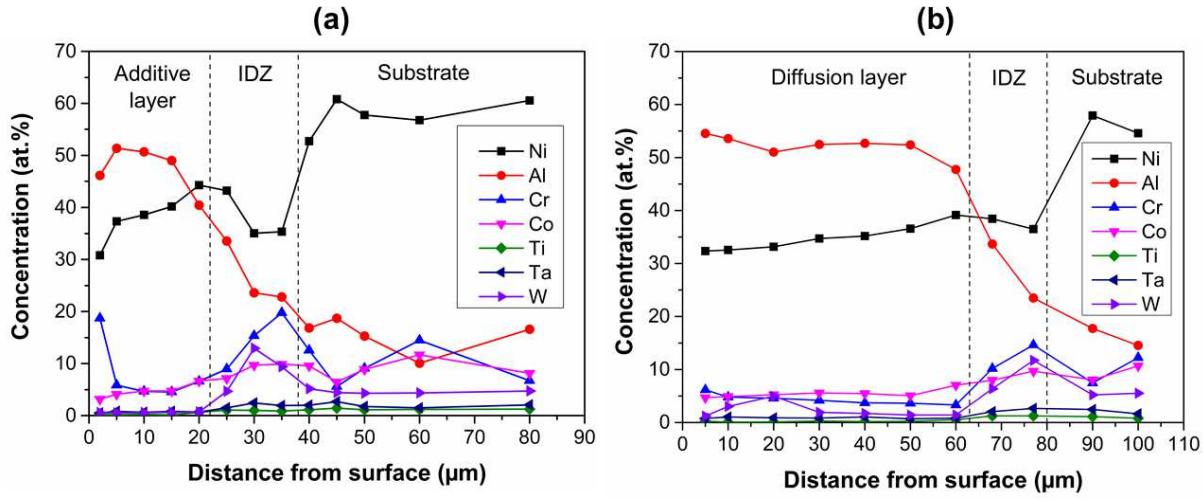

Fig. 7. EDS concentration profiles of the diffusion coatings elaborated on CM-247 LC superalloy from the **(a)** 56Cr/44Al and **(b)** 33Cr/67Al double-layer systems after 400°C-1 h + 700°C-2 h + 1100°C-2 h in flowing Ar.

Further analyses were conducted by SEM on representative areas of the diffusion coatings (**Fig. 8**). For the 56Cr/44Al double-layer system (**Fig. 8**a), the BSE mode points out the incorporation of the substrate carbides within the interdiffusion zone. The additive layer contains many α-(Cr) precipitates whereas Ta is confined within the IDZ. For the 33Cr/67Al system (**Fig. 8**b), Ta-rich bright phases identified as the substrate carbides are present across the whole thickness of the diffusion layer. Unlike the Cr-rich composition, Ta-rich precipitates are also observed in the outer region of the diffusion layer. This confirms that inward diffusion of Al occurred at low temperature. A fine dispersion of α-(Cr) was also observed within the diffusion layer (cf. Cr X-ray map in **Fig. 8**b). This probably resulted from the low solubility of Cr in Al-rich β-NiAl [58].

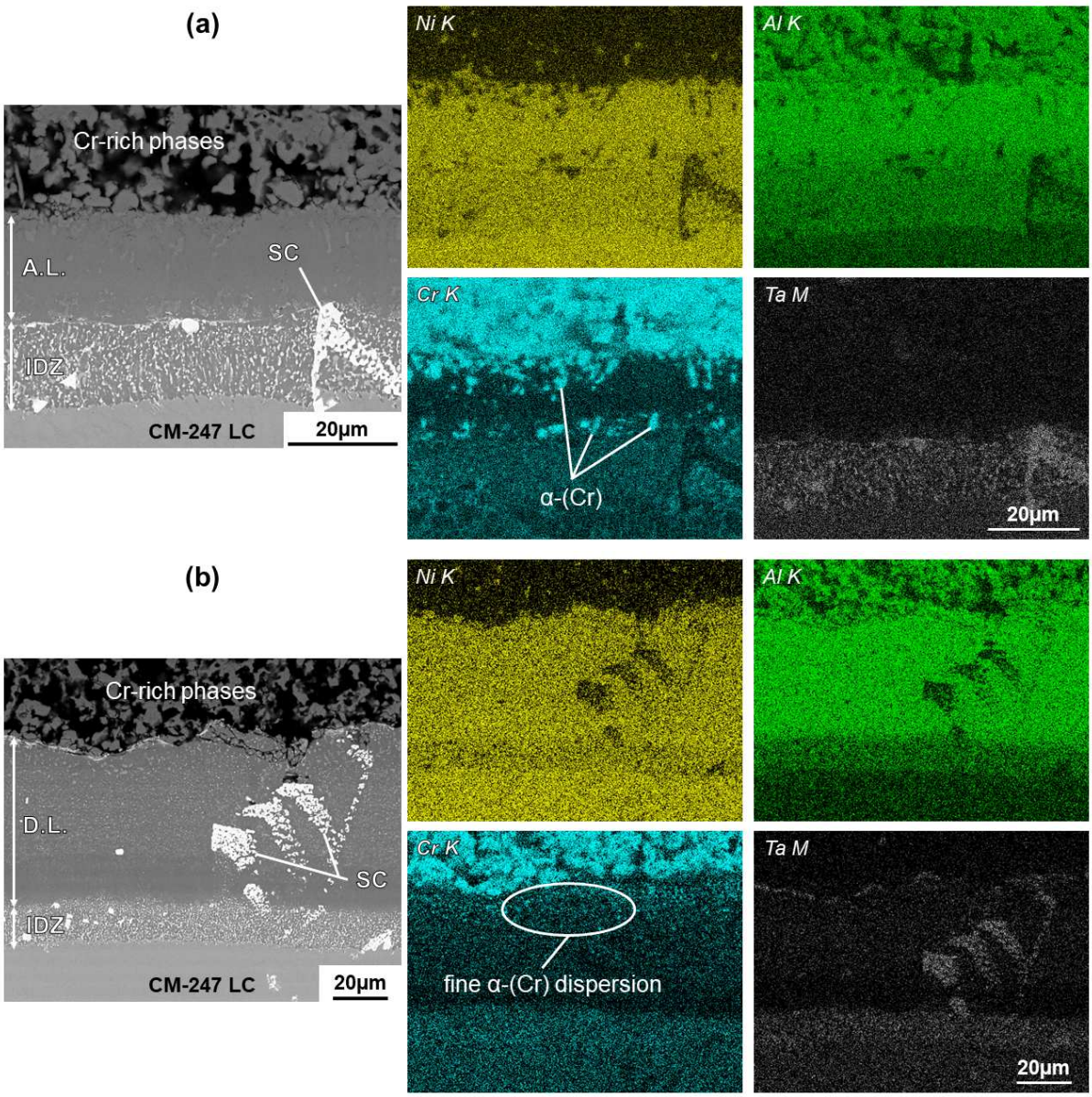

Fig. 8. BSE cross-section image and corresponding X-ray maps of Ni, Al, Cr and Ta for the **(a)** 56Cr/44Al and **(b)** 33Cr/67Al double-layer systems elaborated on CM-247 LC superalloy after 400°C-1 h + 700°C-2 h + 1100°C-2 h in flowing Ar.

4. Discussion

4.1. Mechanisms of formation of the aluminide coatings on Ni20Cr

Whereas Ni-Cr alloys are easily aluminized by pack cementation processes [46-48,52], the high concentration of Cr in the Ni20Cr substrate was found to considerably affect the mechanisms of formation of the diffusion layers from Al-containing water-based slurries [49]. When Al microparticles are in direct contact with Ni20Cr (**Fig. 9**a), wetting and dissolution of the substrate initiate at a temperature slightly lower than the theoretical melting point of Al (e.g. Al-Ni eutectic at about 640°C in Ar [44]). The aluminizing progress is therefore restricted by the availability of Al at the reaction front, the amount of exothermic heat liberated and the heat loss to the surroundings. When molten Al becomes saturated in Ni and/or Cr, the formation of Al-rich intermetallic compounds starts at the reaction front (**Fig. 9**b), which further release heat because of the exothermic nature of the reaction. This, in turn, fosters the liberation of molten Al from the microparticles forming an Al-melt network in the slurry deposit [35,44]. The temperature continues to rise at the interface with the substrate and different intermetallics can form (their stoichiometry depends on the maximum temperature reached during the process). The systematic observation of a Cr-rich layer at the interface between the diffusion spots and the Ni20Cr substrate (**Fig. 1**b) therefore indicates that the Cr-rich intermetallic compounds formed were stable at 700°C and impeded further Al ingress towards the substrate. This caused the formation of diffusion spots (i.e. island like morphology [49]) because of the continuous Al supply from the slurry deposit (**Fig. 9**c). This also provoked the detachment of the top coat composed of hollow alumina spheres as reported by Rannou et al. [49]. The final annealing step at 1100°C for 2 h then promoted the outward diffusion of nickel, which converted the Al-rich Ni_xAl_y phases into β-NiAl and γ'-Ni_3Al (**Fig. 9**d). However, the segregation of Cr was still observed at the reaction front in the form of large α-Cr phases.

For the new slurry coating design (**Fig. 9**a), molten Al reacts with the Cr microparticles forming Al_xCr_y intermetallic phases in the slurry deposit (**Fig. 9**f) as summarized in equation ***(1)***:

$$X_{Al} * Al + (1-X_{Al}) * Cr \rightarrow Al_xCr_y \qquad \textbf{(1)}$$

Where X_{Al} corresponds to the Al activity (i.e. atomic fraction of Al in the initial double-layer system).

The layer of Cr microparticles therefore acted as a barrier of diffusion for Al and the exothermic reactions usually observed between Al and Ni were thus totally suppressed [43]. After the diffusion step (700°C-2 h), the whole reservoir of Al reacted with Cr resulting in a top layer with hollow alumina spheres (**Fig. 9**g). Upon further annealing at 1100°C, the simultaneous outward diffusion of Ni from the substrate and inward diffusion of Al from the synthesized Al_xCr_y phases resulted in the direct formation of β-NiAl at the boundary (**Fig. 9**h). The extensive outward

diffusion of Ni is emphasized with the formation of Kirkendall voids and of a thin Cr-rich IDZ (**Fig. 2**d). Similar microstructures were obtained with a high-temperature low-activity CVD process on Ni20Cr substrate [59]. Whereas the Al donors (i.e. aluminizing residues) were still observed at the surface (**Fig. 9**h), undissolved Cr particles remained in the outer region of the aluminide coating. This opens new perspectives for the elaboration of Cr-modified aluminide coatings based on β-NiAl + α-Cr composites [5,13,58].

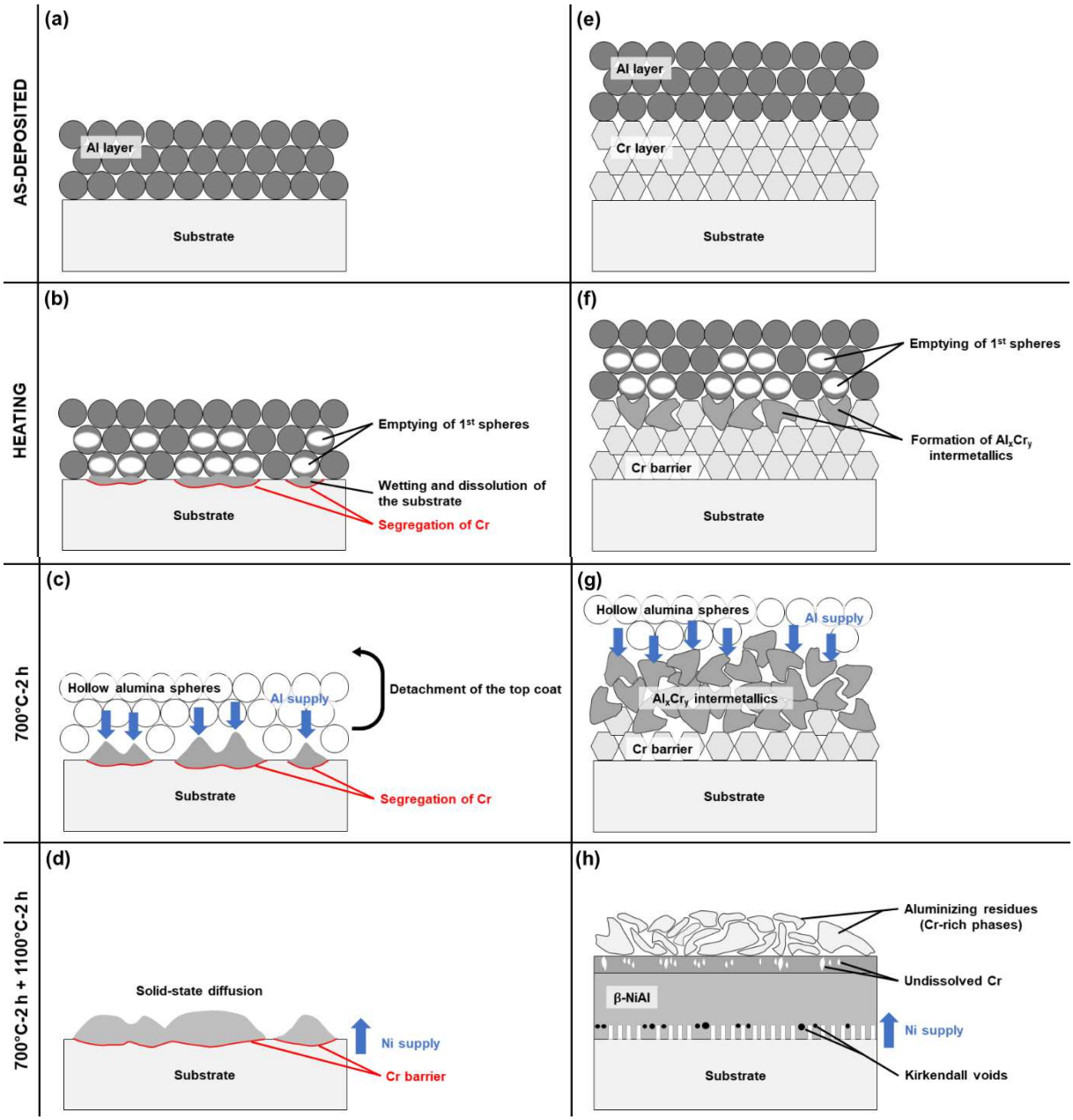

Fig. 9. Schematic of the mechanisms of formation of the aluminide coatings on Ni20Cr substrate from **(a, b, c, d)** Al microparticles and **(e, f, g, h)** the Cr/Al double-layer system.

4.2. Mechanisms of formation of the aluminide coatings on CM-247 LC superalloy

The aluminizing of CM-247 LC superalloy from Al microparticles formed a typical high-activity coating (**Fig. 5**a) resulting from the fast dissolution of the substrate in molten Al and subsequent inward diffusion of Al towards the substrate [44]. Unlike Ni20Cr substrate, continuous diffusion layers were formed on CM-247 LC superalloy. This can be attributed to the lower Cr concentration of the substrate, which prevented the segregation of Cr at the reaction front. However, the inward growth of the coating provoked the embedding of the substrate carbides and the precipitation of slowly-diffusing elements in the diffusion layer [1,4,20,25]. Upon annealing at 1100°C for 2 h, an IDZ grew by outward diffusion of Ni. This heat treatment also converted the δ-Ni_2Al_3 phase into β-NiAl phase [1,4].

With the Cr/Al double-layer system, the initial Cr/Al ratio was found to considerably influence the coating microstructure, i.e. the coating growth direction. In **Fig. 10**a, the substrate carbides are embedded in the IDZ. This indicates that the initial surface of the substrate corresponds to the interface between the IDZ and the additive layer and that the coating formed by predominant outward diffusion of Ni at high-temperature (i.e. 1100°C) [1,4,20]. Because of the Ni withdrawal from the substrate, an IDZ grows with an IDZ/A.L. thickness ratio close to one.

As given in equation ***(1)***, molten Al first reacts with Cr to form Al_xCr_y intermetallic phases at approximately 640°C [45]. This considerably reduces the Al activity on the substrate surface and slows down the inward diffusion of Al towards the substrate during the diffusion step (700°C-2 h). The further annealing at 1100°C for 2 h fosters the outward diffusion of Ni and its combination with Al coming from the synthesized Al_xCr_y phases. Since Ni has a low solubility in the Al-Cr phases (about 1 at.% in Al_4Cr and 3 at.% in Al_8Cr_5) [53] and because the formation of Ni_xAl_y is more exothermic than that of Ni_xCr_y phases, Ni preferentially combines with Al and the Al-Cr phases become progressively richer in Cr. This fostered the formation of an outwardly growing Ni-rich β-NiAl layer with a large fraction of undissolved Cr given its limited solubility in the β-NiAl phase (less than 8 at.% at 1100°C [58]). This highlights that the outward diffusion rate of Ni was significantly higher than the inward diffusion rate of Al at all time during the aluminizing process [5,13].

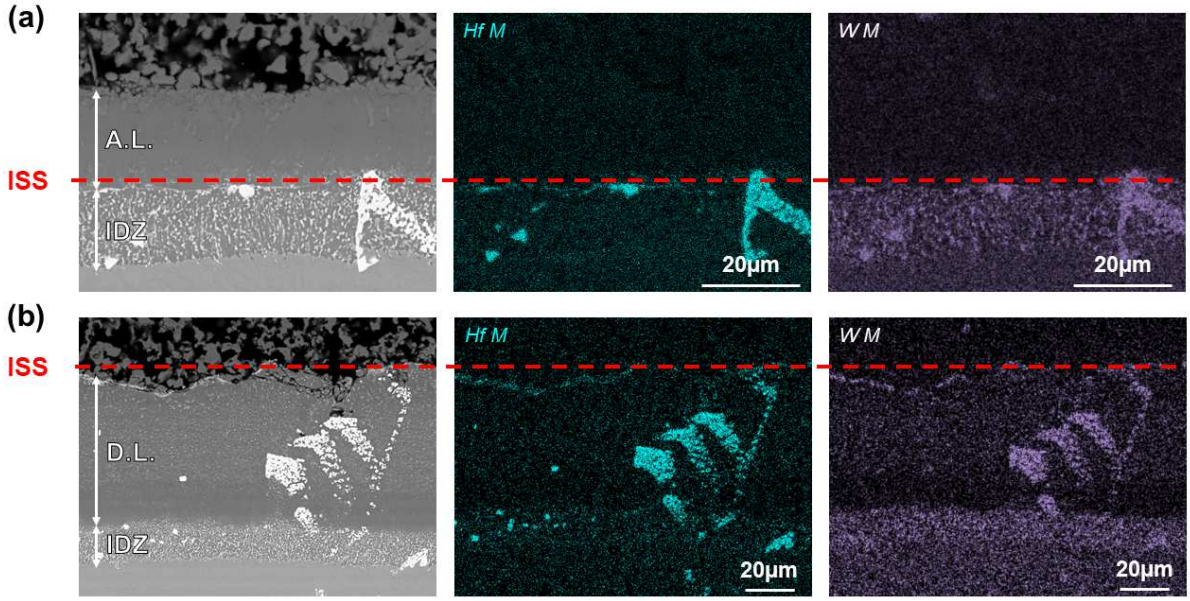

Fig. 10. BSE cross-section images and corresponding X-ray maps of Hf and of W for the aluminide coatings formed on CM-247 LC superalloy with the **(a)** 56Cr/44Al and **(b)** 33Cr/67Al double-layer systems. The initial surface of the substrate (ISS) is highlighted with the position of the substrate carbides after the aluminizing process.

For the 33Cr/67Al system (**Fig. 10**b), the substrate carbides are observed across the whole thickness of the coating. This indicates that the initial surface of the substrate remained at the outermost surface of the coating and that inward diffusion of Al towards the substrate was predominant [20]. This could also indicate that the thickness of the Cr layer (**Table *2***) was too thin and that molten Al reacted with the substrate initiating the aluminizing process at low temperature. This highlights the influence of the thermodynamic activity of Al (i.e. the initial Cr/Al ratio) on the final microstructure of the coatings [60]. One of our previous works demonstrated that both the intensity of the exothermic reactions between Al and Cr microparticles and the stoichiometry of the Al-Cr intermetallic phases formed are a direct consequence of the initial Cr/Al ratio [45]. It was previously shown that for the 67Al33Cr composition (in wt.%), Al had reacted with Cr after only 10 minutes at 650°C resulting in $Al_{11}Cr_2$ and Al_4Cr intermetallic phases [45,61]. This implies that the annealing of the Cr/Al double-layer at 700°C for 2 h may have led to the complete reaction between the Al and the Cr layers so that the excess molten Al and/or the Al_4Cr phases may have reacted further with the substrate. The further annealing at 1100°C fostered the outward diffusion of Ni and converted the δ-Ni_2Al_3 phase into β-NiAl as observed in the high-activity coatings.

5. Conclusions

Based on this work, the following conclusions can be drawn:

1. Aluminizing of Ni20Cr from Al-containing water-based slurries involved the simultaneous dissolution of the substrate in molten Al and segregation of Cr at the reaction front. The formation of a Cr-rich layer at the reaction front impeded further Al ingress into the substrate. Increasing the temperature to 1100°C promoted the outward diffusion of Ni from the substrate and the conversion of the Al-rich Ni_xAl_y phases into β-NiAl and γ'-Ni_3Al.
2. Incorporating a layer of Cr microparticles between the substrate and Al microparticles modified the mechanisms of aluminizing of Ni20Cr. The Cr interlayer acted as a barrier to molten Al by forming Al_xCr_y intermetallic phases in the slurry deposit. This prevented the highly exothermic reaction between molten Al and Ni20Cr and the dissolution of the latter. Alternatively, the formation of Al_xCr_y phases decreased the thermodynamic activity of Al and considerably reduced the Al inward diffusion at 700°C. A further annealing at 1100°C for 2 h fostered the Ni outward diffusion and the direct formation of β-NiAl at the boundary between the substrate and the Al_xCr_y phases. This resulted in a β-NiAl coating matrix with undissolved Cr in the outer layer.
3. By adjusting the initial composition of the double-layer system (i.e. thicknesses of Cr and Al layers), both low-activity and high-activity coating microstructures were obtained on CM-247 LC superalloy. The threshold to achieve low-activity coating microstructures on CM-247 LC was between 56Cr/44Al and 33Cr/67Al compositions. In this study, low-activity coatings were obtained even when performing the same two-step heat treatment (700°C-2 h + 1100°C-2 h) employed for the high-activity coatings.
4. The outwardly-growing coatings exhibit an additive layer based on β-NiAl with α-(Cr) and, unlike inwardly-growing coatings, the deleterious elements for oxidation resistance (e.g. Mo, W, Ta) remained in the interdiffusion zone after aluminizing.

This new slurry coating design offers new opportunities to coat gas turbine components with complex geometry. The oxidation and hot corrosion resistance of these coatings should also be evaluated.

Acknowledgements

The authors gratefully acknowledge the French Ministry of Armed Forces (Direction Générale de l'Armement) for funding this research (Grant no. 2014.60.0059).

References

[1] G.W. Goward, Current Research on the Surface Protection of Superalloys for Gas Turbine Engines, JOM 22 (1970) 31-39.

[2] J. Stringer, High-temperature corrosion of superalloys, Mater. Sci. Technol. 3 (1987) 482-493.

[3] J.R. Nicholls, Designing Oxidation-Resistant Coatings, JOM 52 (2000) 28-35.

[4] G.W. Goward, D.H. Boone, Mechanisms of Formation of Diffusion Aluminide Coatings on Nickel-Base Superalloys, Oxid. Met. 3 (1971) 475-495.

[5] R. Streiff, D.H. Boone, Corrosion Resistant Modified Aluminide Coatings, J. Mater. Eng. Perf. 22 (2013) 2801-2812.

[6] M. Thoma, A. Scrivani, C. Giolli, A. Giorgetti, Aluminizing Turbine Parts – Processes and Coatings, Proceedings of ASME Turbo Expo 2011, Vancouver, British Columbia, Canada (2011) 783-789.

[7] D.K. Das, Microstructure and high temperature oxidation behavior of Pt-modified aluminide bond coats on Ni-base superalloys, Prog. Mater. Sci. 58 (2013) 151-182.

[8] M.W. Brumm, H.J. Grabke, The Oxidation Behaviour of NiAl – I. Phase Transformations in the Alumina Scale During Oxidation of NiAl and NiAl-Cr Alloys, Corr. Sci. 33 (1992) 1677-1690.

[9] H.J. Choi, J. Jedlinski, B. Yao, Y.H. Sohn, Transmission electron microscopy observations on the phase composition and microstructure of the oxidation scale grown on as-polished and yttrium-implanted β-NiAl, Surf. Coat. Technol. 205 (2010) 1206-1210.

[10] R. Swadźba, M. Hetmańczyk, J. Wiedermann, L. Swadźba, G. Moskal, B. Witala, K. Radwański, Microstructure degradation of simple, Pt- and Pt+Pd-modified aluminide coatings on CMSX-4 superalloy under cyclic oxidation conditions, Surf. Coat. Technol. 215 (2013) 16-23.

[11] G.W. Goward, L.W. Cannon, Pack Cementation Coatings for Superalloys: a Review of History, Theory, and Practice, J. Eng. Gas Turb. Power 110 (1988) 150-154.

[12] R.E. Malush, P. Deb, D.H. Boone, Structure and 900 °C Hot Corrosion Behavior of Chromium-Modified Platinum Aluminide Coatings, Surf. Coat. Technol. 36 (1988) 13-26.

[13] B. Gleeson, W.H. Cheung, W. Da Costa, D.J. Young, The Hot-Corrosion Behavior of Novel Co-Deposited Chromium-Modified Aluminide Coatings, Oxid. Met. 38 (1992) 407-424.

[14] R. Bianco, M.A. Harper, R.A. Rapp, Codepositing Elements by Halide-Activated Pack Cementation, JOM 43 (1991) 68-73.

[15] K. Shirvani, M. Saremi, A. Nishikata, T. Tsuru, Electrochemical study on hot corrosion of Si-modified aluminide coated In-738LC in Na_2SO_4–20 wt.% NaCl melt at 750 °C, Corr. Sci. 45 (2003) 1011-1021.

[16] V.K. Tolpygo, D.R. Clarke, Rumpling of CVD (Ni,Pt)Al diffusion coatings under intermediate temperature cycling, Surf. Coat. Technol. 203 (2009) 3278-3285.

[17] N. Eliaz, G. Shemesh, R.M. Latanision, Hot corrosion in gas turbine components, Eng. Fail. Anal. 9 (2002) 31-43.

[18] R. Rajendran, Gas turbine coatings – An overview, Eng. Fail. Anal. 26 (2012) 355-369.

[19] S. Dryepondt, J.R. Porter, D.R. Clarke, On the initiation of cyclic oxidation-induced rumpling of platinum-modified nickel aluminide coatings, Acta Materialia 57 (2009) 1717-1723.

[20] D.K. Das, V. Singh, S.V. Joshi, Evolution of Aluminide Coating Microstructure on Nickel-Base Cast Superalloy CM-247 in a Single-Step High-Activity Aluminizing Process, Metall. Mater. Trans. A 29 (1998) 2173-2188.

[21] G.F. Slattery, Microstructural aspects of aluminized coatings on nickel-base alloys, Met. Technol. 10 (1983) 41-51.

[22] S. Shankar, L.L. Seigle, Interdiffusion and Intrinsic Diffusion in the NiAl (δ) Phase of the Al-Ni System, Metall. Trans. A 9 (1978) 1467-1477

[23] J.M. Brossard, B. Panicaud, J. Balmain, G. Bonnet, Modelling of aluminized coating growth on nickel, Acta Materialia 55 (2007) 6586-6595.

[24] J. Angenete, K. Stiller, Comparison of inward and outward grown Pt modified aluminide diffusion coatings on a Ni based single crystal superalloy, Surf. Coat. Technol. 150 (2002) 107-118.

[25] Z.D. Xiang, J.S. Burnell-Gray, P.K. Datta, Aluminide coating formation on nickel-base superalloys by pack cementation process, J. Mater. Sci. 36 (2001) 5673-5682.

[26] J. Angenete, K. Stiller, E. Bakchinova, Microstructural and microchemical development of simple and Pt-modified aluminide diffusion coatings during long term oxidation at 1050 °C, Surf. Coat. Technol. 176 (2004) 272-283.

[27] F. Bozza, G. Bolelli, C. Giolli, A. Giorgetti, L. Lusvarghi, P. Sassatelli, A. Scrivani, A. Candeli, M. Thoma, Diffusion mechanisms and microstructure development in pack aluminizing of Ni-based alloys, Surf. Coat. Technol. 239 (2014) 147-159.

[28] J. Benoist, K.F. Badawi, A. Malié, C. Ramade, Microstructure of Pt modified aluminide coatings on Ni-based superalloys without prior Pt diffusion, Surf. Coat. Technol. 194 (2005) 48-57.

[29] Y.Q. Wang, G. Sayre, Factors affecting the microstructure of platinum-modified aluminide coatings during a vapor phase aluminizing process, Surf. Coat. Technol. 203 (2009) 1264-1272.

[30] M. Zagula-Yavorska, J. Romanowska, M. Pytel, J. Sieniawski, The microstructure and oxidation resistance of the aluminide coatings deposited by the CVD method on pure nickel and hafnium-doped nickel superalloys, Arch. Civ. Mech. Eng. 15 (2015) 862-872.

[31] A.J. Rasmussen, A. Agüero, M. Gutierrez, M.J. Landeira Østergård, Microstructures of thin and thick slurry aluminide coatings on Inconel 690, Surf. Coat. Technol. 202 (2008) 1479-1485.

[32] X. Montero, M.C. Galetz, M. Schütze, A single step process to form in-situ an alumina foam/aluminide TBC system for alloys in extreme environments at high temperatures, Surf. Coat. Technol. 206 (2011) 1586-1594.

[33] B. Rannou, F. Velasco, S. Guzmán, V. Kolarik, F. Pedraza, Aging and thermal behavior of a PVA/Al microspheres slurry for aluminizing purposes, Mater. Chem. Phys. 134 (2012) 360-365.

[34] F. Pedraza, M. Mollard, B. Rannou, J. Balmain, B. Bouchaud, G. Bonnet, Potential thermal barrier coating systems from Al microparticles. Mechanisms of coating formation on pure nickel, Mater. Chem. Phys. 134 (2012) 700-705.

[35] B. Bouchaud, B. Rannou, F. Pedraza, Slurry aluminizing mechanisms of Ni-based superalloys incorporating an electrosynthesized ceria diffusion barrier, Mater. Chem. Phys. 143 (2013) 416-424.

[36] X. Montero, M.C. Galetz, M. Schütze, Low-activity aluminide coatings for superalloys using a slurry process free of halide activators and chromates, Surf. Coat. Technol. 222 (2013) 9-14.

[37] B. Rannou, B. Bouchaud, J. Balmain, G. Bonnet, F. Pedraza, Comparative Isothermal Oxidation Behaviour of New Aluminide Coatings from Slurries Containing Al Particles and Conventional Out-of-Pack Aluminide Coatings, Oxid. Met. 81 (2014) 139-149.

[38] F. Pedraza, M. Mollard, B. Rannou, B. Bouchaud, J. Balmain, G. Bonnet, Oxidation Resistance of Thermal Barrier Coating Based on Hollow Alumina Particles, Oxid. Met. 85 (2016) 231-244.

[39] M. Mollard, F. Pedraza, B. Bouchaud, X. Montero, M.C. Galetz, M. Schütze, Influence of the superalloy substrate in the synthesis of the Pt-modified aluminide bond coat made by slurry, Surf. Coat. Technol. 270 (2015) 102-108.

[40] X. Montero, M.C. Galetz, M. Schütze, Sulphidation Behavior of a Non Harmful Water-Based Al and Al-Si Slurry Coating on CM247 Superalloy, Oxid. Met. 80 (2013) 635-649.

[41] X. Montero, M.C. Galetz, M. Schütze, A Novel Type of Environmentally Friendly Slurry Coatings, JOM 67 (2014) 77-86.

[42] C. Boulesteix, F. Pedraza, M. Proy, I. Lasanta, T. de Miguel, A. Illana, F.J. Pérez, Steam Oxidation Resistance of Slurry Aluminum and Aluminum/Silicon Coatings on Steel for Ultrasupercitical Steam Turbines, Oxid. Met. 87 (2017) 469-479.

[43] B. Grégoire, G. Bonnet, F. Pedraza, Mechanisms of formation of slurry aluminide coatings from Al and Cr microparticles, Surf. Coat. Technol. 359 (2019) 323-333.

[44] M.C. Galetz, X. Montero, M. Mollard, M. Gunthner, F. Pedraza, M. Schütze, The role of combustion synthesis in the formation of slurry aluminization, Intermetallics 44 (2014) 8-17.

[45] B. Grégoire, G. Bonnet, F. Pedraza, Reactivity of Al-Cr microparticles for aluminizing purposes, Intermetallics 81 (2017) 80-89.

[46] D.C. Tu, L.L. Seigle, Kinetics of formation and microstructure of aluminide coatings on Ni-Cr alloys, Thin Solid Films 95 (1982) 47-56.

[47] H.L. Huang, Y.Z. Chen, D. Gan, Microstructure of first-stage aluminized coating on a Ni–Cr alloy, Mater. Sci. Eng. A 328 (2002) 238-244.

[48] H.L. Huang, D. Gan, Microstructure of aluminized coating on a Ni–Cr alloy after annealing treatment, Mater. Sci. Eng. A 485 (2008) 550-557.

[49] B. Rannou, B. Bouchaud, J. Balmain, V. Kolarik, F. Pedraza, On the Influence of a Heat Treat for an Aluminizing Progress Based on Al Microparticles Slurry for Model Ni and Ni20Cr. Experimental and Theoretical Approaches, Defect Diff. Forum 323-325 (2012) 373-379.

[50] B. Grushko, W. Kowalski, D. Pavlyuchkov, S. Mi, M. Surowiec, Al-rich region of the Al–Ni–Cr alloy system below 900 °C, J. Alloys Compd. 485 (2009) 132-138.

[51] Y. Wang, G. Cacciamani, Thermodynamic modeling of the Al-Cr-Ni system over the entire composition and temperature range, J. Alloys Compd. 688 (2016) 422-435.

[52] D. Erdeniz, D.C. Dunand, Microstructure development during pack aluminization of nickel and nickel-chromium wires, Intermetallics 50 (2014) 43-53.

[53] B. Grushko, W. Kowalski, D. Pavlyuchkov, B. Przepiorzynski, M. Surowiec, A contribution to the Al–Ni–Cr phase diagram, J. Alloys Compd. 460 (2008) 299-304.

[54] W. Huang, Y.A. Chang, Thermodynamic properties of the Ni-Al-Cr system, Intermetallics 7 (1999) 863-874.

[55] N. Ta, L. Zhang, Y. Tang, W. Chen, Y. Du, Effect of temperature gradient on microstructure evolution in Ni–Al–Cr bond coat/substrate systems: A phase-field study, Surf. Coat. Technol. 261 (2015) 364-374.

[56] A.J. Bradley, A. Taylor, An X-Ray Analysis of the Nickel-Aluminium System, Proc. Roy. Soc. A 159 (1937) 56-72.

[57] J.J. Rechtien, C.R. Kannewurf, J.O. Brittain, Optical Constants of β-Phase NiAl, J. Appl. Phys. 38 (1967) 3045-3050.

[58] W.H. Tian, C.S. Han, M. Nemoto, Precipitation of α-Cr in B2-ordered NiAl, Intermetallics 7 (1999) 59-67.

[59] Y. Le Guevel, B. Grégoire, B. Bouchaud, P. Bilhé, A. Pasquet, M. Thiercelin, F. Pedraza, Influence of the oxide scale features on the electrochemical descaling and stripping of aluminide coatings, Surf. Coat. Technol. 292 (2016) 1-10.

[60] J. Grüters, M.C. Galetz, Influence of thermodynamic activities of different masteralloys in pack powder mixtures to produce low activity aluminide coatings on TiAl alloys, Intermetallics 60 (2015) 19-27.

[61] K. Naplocha, K. Granat, Combustion synthesis of Al–Cr preforms activated in microwave field, J. Alloys Compd. 480 (2009) 369-375.